

Design and evaluation of a deformable multi-organ abdominal phantom for multimodality imaging applications

† Mandy Yuan ^{a,b}, † Nati Nawawithan ^{a,b}, James Yu ^{a,c}, Chinmay Patwardhan ^{a,b},
Suhani Swain ^{a,b}, Izabella Chaverra ^{a,b}, Baowei Fei ^{a,b,c}*

^a Center for Imaging and Surgical Innovation, University of Texas at Dallas, Richardson, TX

^b Department of Bioengineering, University of Texas at Dallas, Richardson, TX

^c Department of Radiology, University of Texas Southwestern Medical Center, Dallas, TX

† Equal contribution, * Corresponding author: bfei@utdallas.edu, Website: <https://fei-lab.org>

ABSTRACT

A deformable multi-organ abdominal phantom can have many applications in medical imaging and image-guided interventions. It can provide ground truth data for registration evaluation and procedure training. In this study, we designed and fabricated a deformable abdominal phantom for multimodal imaging applications. Computed tomography (CT) images of a human patient were used to segment the abdominal surface, kidneys, spleen, and liver. Scaled down 3D-printed molds were created based on the segmented 3D models of these structures. To allow for deformability, an agar-gelatin gel mixture was used to cast the phantom using the 3D-printed molds with potassium iodide added to the target formulation as a CT contrast agent. Psyllium husk powder was utilized as an ultrasound (US) scattering agent. Simulated tumors or targets were incorporated into the kidney phantom. All components were assembled into an abdominal mold to replicate patient anatomical structures. The phantom was evaluated using CT and ultrasound imaging, with preliminary results demonstrating its ability to provide ground truth for tumor localization. This study presents a reproducible framework for creating a deformable abdominal phantom that can be applied to the development and validation of image-guided interventional procedures.

Keywords: Deformable phantom, multi-modality imaging, minimally invasive interventions, ultrasound imaging, CT

1. INTRODUCTION

Tissue-mimicking phantoms (TMPs) play a critical role in the development, calibration, and validation of imaging systems and therapeutic procedures in medical practice.¹ These constructs are engineered to replicate the anatomical geometry, mechanical properties, and imaging signatures of biological tissues, thereby enabling realistic, repeatable, controlled experimentation for translational biomedical research.² Specifically, water-based materials' properties for TMP production, such as agar and gelatin, have been comparable to human tissue.³ For image-guided interventions,⁴ phantoms provide non-invasive, risk-free surrogate targets for assessing image system performance and procedural accuracy across the various imaging modalities.⁵

Despite their growing applications in image-guided interventions, phantoms have presented trade-offs that limit broader experimental applications. Commercial phantoms can be expensive and often portray simpler anatomy or geometry, restricting representation of the variability of clinical scenarios that can be studied.^{6,7} Especially for image-guided interventions where target size, shape, and location are crucial factors to accurately understanding varied pathology, customizable and low-cost phantoms can greatly improve experimental breadth and biomedical discovery. Additionally, traditional materials often require complex fabrication processes⁸ or are optimized for single imaging modalities. Hydrogel-based materials enable in-house tailored phantom creation with low-cost reagents and simple techniques, offering more opportunities to explore complex anatomy and train multimodal imaging to better understand how to improve clinical intervention implementation.

Beyond interventional use, TMPs have been adapted for specialized pre-clinical imaging applications. In a previous work from our group, polyvinyl chloride-based phantoms offer low-cost, dual-modality compatibility for CT and US imaging, showcasing these phantoms as a valuable step in renal procedure planning and hybrid imaging system calibration.⁹ Optical tissue-mimicking phantoms fabricated from agar, intralipid, and absorbing dyes provide controlled scattering and absorption coefficients, enabling standardized performance evaluation of biomedical optical imaging systems and future

usage in tissue property analysis.¹⁰ Multi-biomarker-optimized phantoms extend these capabilities by incorporating chromophores and fluorophores to replicate complex tissue optical signatures, supporting spectroscopy-based diagnostics.¹¹ Recent advances in additive manufacturing have further enhanced TMP realism. Three-dimensional (3D) printed CT phantoms using iodine-based inks enable radiomics feature extraction with precise spatial control of contrast patterns, improving quantitative imaging validation.¹² Collectively, these developments highlight the versatility of TMPs across imaging modalities and therapeutic platforms, underscoring their essential role in bridging pre-clinical research and clinical translation.

The goal of this study is to design a deformable, customized abdominal phantom that can be evaluated across different medical imaging modalities to support deformable registration and other computer vision algorithm evaluations. Phantom design aims to facilitate low-cost production and tailored, anthropomorphic accuracy through molds based on CT images of real patients.

2. MATERIALS AND METHODS

2.1 Materials

Two categories of tissue-mimicking materials, gelatin-based gels and agar-based gels, were applied through components of the whole-abdominal phantoms, including the kidney phantoms and tumor inserts. Gelatin A (175 Bloom, Sigma-Aldrich) and agar powder (Sigma-Aldrich) served as the primary gelling agents. Both materials were hydrated in deionized water and heated until fully dissolved, then allowed to cool under controlled conditions to form solid hydrogels. Glycerol (Fisher Scientific) was incorporated into both gelatin- and agar-based formulations to increase mechanical strength and reduce brittleness, as well as to better mimic the elastic properties of soft tissue. Different concentrations were evaluated to determine formulations that provided higher physical stability.

To provide tunable X-ray attenuation for CT imaging, potassium iodide (KI) solutions of varying concentrations (1–3% w/v) were prepared and incorporated into the gel mixtures prior to casting. The iodinated gels were both used in localized tumor inserts in specific regions of the kidney and abdominal phantom to simulate contrast-enhanced tissues. To provide acoustic reflection for US imaging, psyllium husk powder (1.6–3.2% w/v) was added to both tumor and internal structures. All materials used were commercially available and prepared in-house immediately prior to phantom fabrication to minimize dehydration and ensure uniform material properties.

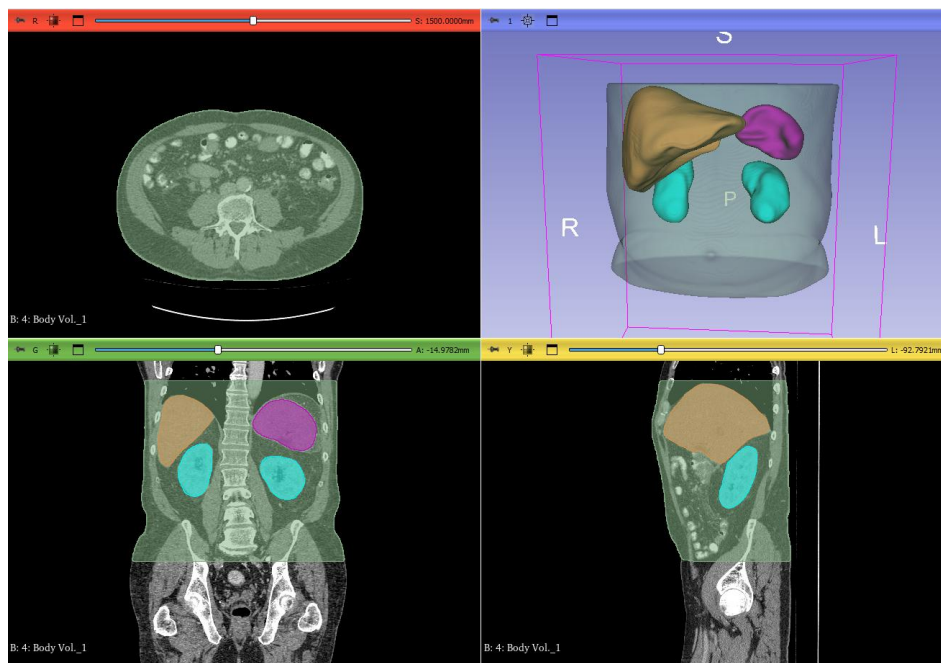


Figure 1. Segmented components of the abdominal phantom from the CT image. The components are abdominal surface (green), liver (orange), spleen (purple), and two kidneys (blue).

2.2 Phantom Workflow

The deformable abdominal phantom consists of the abdominal surface, two kidneys with inserted targets, the liver, and the spleen. A CT image in the DICOM format was imported into the 3D slicer software, and each component of the phantom was segmented as shown in Figure 1.

Following segmentation, the organ meshes contained well over 100,000 surface facets that were simplified in Autodesk Fusion 360 using feature-preserving decimation and light smoothing to remove non-anatomical irregularities. To fit the volume of the 3D printer, the model was uniformly scaled to approximately 43% of its original physical dimensions.

Molds were generated using a modular insert-plate design. Each organ geometry was used to subtract its shape from basic solid blocks sized to the nearest millimeter, forming negative cavities for casting.

To allow accurate casting of asymmetric internal structures, an internal organ-positioning plate was incorporated as seen in Figure 2. Organs were digitally split at the plate interface, offset by the plate thickness, and the cut surfaces were reconstructed to maintain anatomical continuity.

Proper alignment of the mold halves was ensured using a rectangular tongue-and-groove feature positioned concentrically around the cavity. These edges were rounded to reduce friction and prevent vacuum locking during demolding. The internal surfaces of all molds and the positioning plate were smoothed by progressive sanding with finer grits, followed by final polishing with a rotary tool to support clean, non-destructive release of the gelatin phantoms.

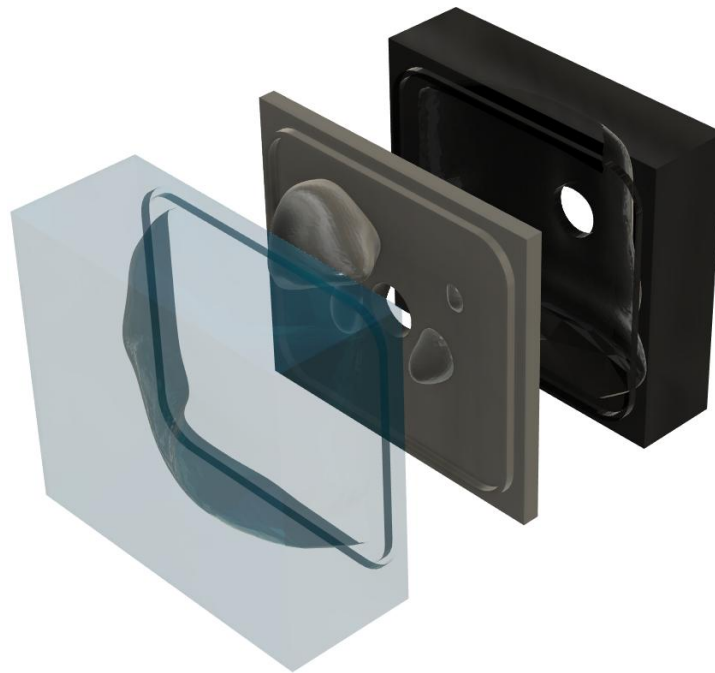


Figure 2. Exploded isometric view in Autodesk Fusion 360 depicting the anterior mold (blue) organ-positioning plate (grey) and posterior mold (black) assembly.

The gelatin solution was prepared with 10% w/v gelatin and 15% v/v glycerol. First, gelatin powder was added to a beaker containing deionized water at room temperature. The mixture was stirred to form a hydrated granular slurry. Subsequently, the slurry was heated in a microwave until it reached a boil. The heated solution was stirred using a magnetic stirrer until it became transparent. To ensure high-fidelity reproduction of the internal cavities, a sequential casting workflow using two identical batches was employed.

All parts of the mold were coated with a thin film of soybean oil to prevent adhesion between the mold and the phantom. In the anterior phase, the organ positioning plate was secured to the anterior mold, and the first batch of gelatin was poured until it reached the brim of the plate.

The posterior mold was attached to the positioning plate. A second batch of gelatin was then poured through its aperture. This allowed the two halves to be joined by a small gelatin bridge passing through the plate's central aperture.

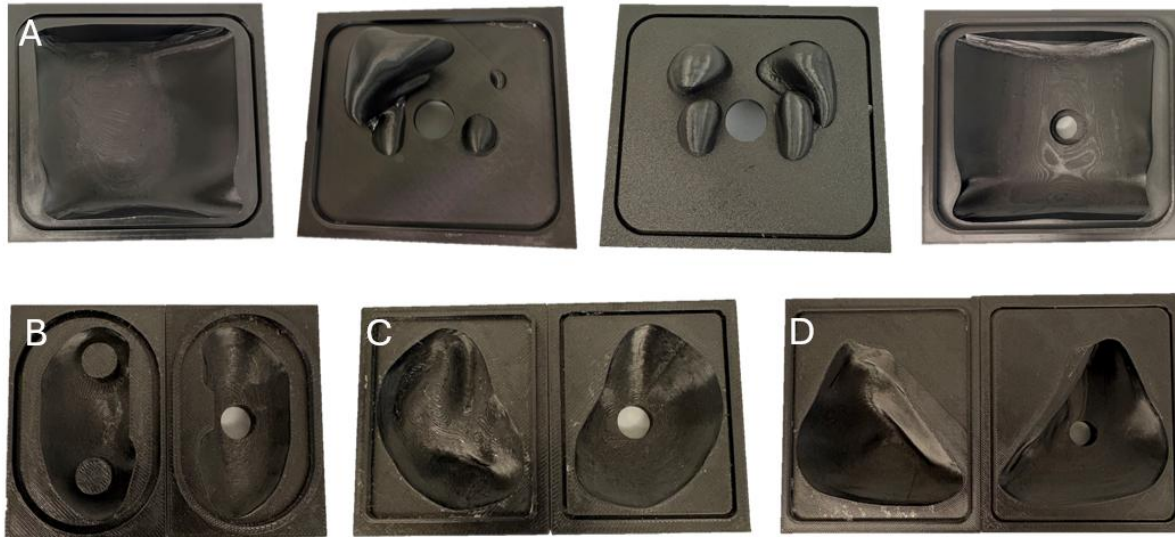


Figure 3. 3D-printed molds and positioning plates for each phantom component. (A) Abdominal cavity components, shown left to right: Anterior mold, anterior side of the organ positioning plate, posterior side of the organ positioning plate, and posterior mold. (B–D) Organ-specific molds showing posterior (left) and anterior (right) sections for the (B) kidney (posterior mold includes negative tumor insertion sites), (C) spleen, and (D) liver.

The solidification and extraction phase included refrigeration at 2-8°C for 18-20 hours and subsequently, leaving the mold assembly at room temperature for an hour to equilibrate, after which the halves were separated. The gelatin bridge at the central aperture was manually sectioned, allowing for the removal of the organ positioning plate.

This process resulted in two discrete abdominal halves with aligned internal voids. The modular design allowed the positioning plate to be reused for multiple casts while ensuring the anatomically accurate placement of the subsequent organ phantoms. Each printed mold and the organ positioning plate can be seen in Figure 3.

The organ phantoms were fabricated utilizing the same 10% w/v gelatin and 15% v/v glycerol solution as the abdomen. Imaging contrast of 0.5% w/v KI and 1.6% w/v psyllium husk powder was added to provide enhanced visualization of the organs when integrated into the abdomen. Targets were created using agar, a firmer hydrogel, to increase structural integrity and provide a stiffness difference for future procedural applications such as biopsy targeting. Experiments testing different concentrations of KI were performed to determine the various Hounsfield unit (HU) ranges that could be produced from KI to mimic various parts of the body such as bone, soft tissue, or fat. A solution of 2% w/v agar and 10% w/v glycerol was mixed with aqueous KI and 3.2% w/v psyllium husk solutions in a 6-well plate. These solutions were set in the 2-8 °C refrigerator to solidify for approximately two hours. Once the targets are solidified, they can be cut into various shapes to be inserted into the organ or abdomen phantom. The phantoms were scanned with the CT (Figure 4).

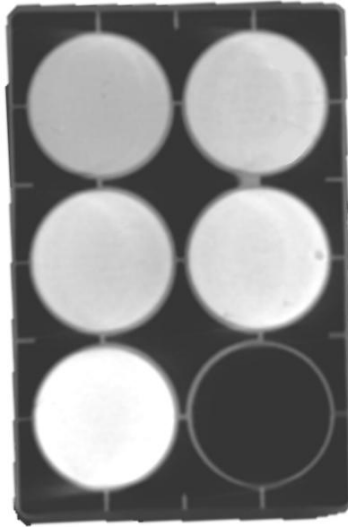


Figure 4. A CT image of tumor phantoms with 3.2% w/v psyllium husk powder and five different concentrations of KI (from left to right), top row: 1.0% w/v and 1.5% w/v, central row: 2.0% w/v and 2.5% w/v, bottom row: 3.0% w/v.

2.3 Methods and Data

Once the phantom fabrication was finished, we validated it with two medical imaging modalities, CT and US. A Ziehm Vision RFD 3D C-arm (Ziehm Imaging Inc., Orlando, FL) was used to acquire CT images of the phantom. 3D slicer software was utilized for CT image visualization and HU measurements of the regions of interest (ROI) in the phantom. The GEM5ScD clinical phased array transducer along with the Verasonics Vantage 256 system (Redmond, WA) and the 5P1 probe along with a BK3000 system (BK Medical Holding Company, MA) were implemented for ultrasound image acquisition of this phantom. Figure 5 shows the experiment setup of both medical imaging modalities in this study.

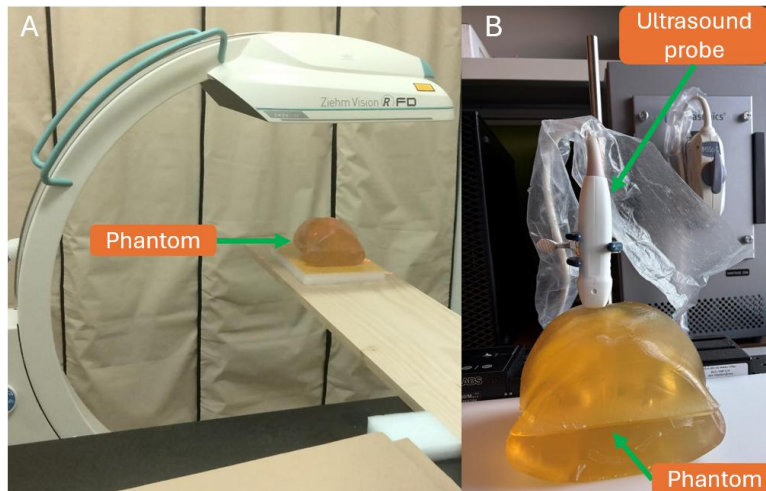


Figure 5. Experiment setup of (A) CT imaging, (B) US imaging.

3. RESULTS

The deformable abdominal phantom accurately replicates the external topography of the abdominal surface. Due to the opacity of the base material and visual homogeneity of the small internal structures, embedded targets are not visible to the naked eye, as shown in Figure 6. Therefore, CT imaging was performed to localize the lesion targets within the phantom. As illustrated in Figure 7, the CT images clearly visualize the internal organs and tumor targets. The 3D reconstructed CT volume highlights the internal structures in yellow, and the tumors in red. Table 1 lists the mean HU values of different KI concentrations in the simulated tumors. The phantom was also imaged using ultrasound systems, demonstrating its suitability for image-guided procedures such as biopsy. Figure 8 presents representative US images of the abdominal phantom, in which the tumor insert is visible as a more hyperechoic region in both the B-mode images from both the GEM5ScD clinical phased array transducer and the 5P1 probe.



Figure 6. Fabricated phantom models of (A) abdominal surface, (B) kidneys, (C) spleen, (D) liver.

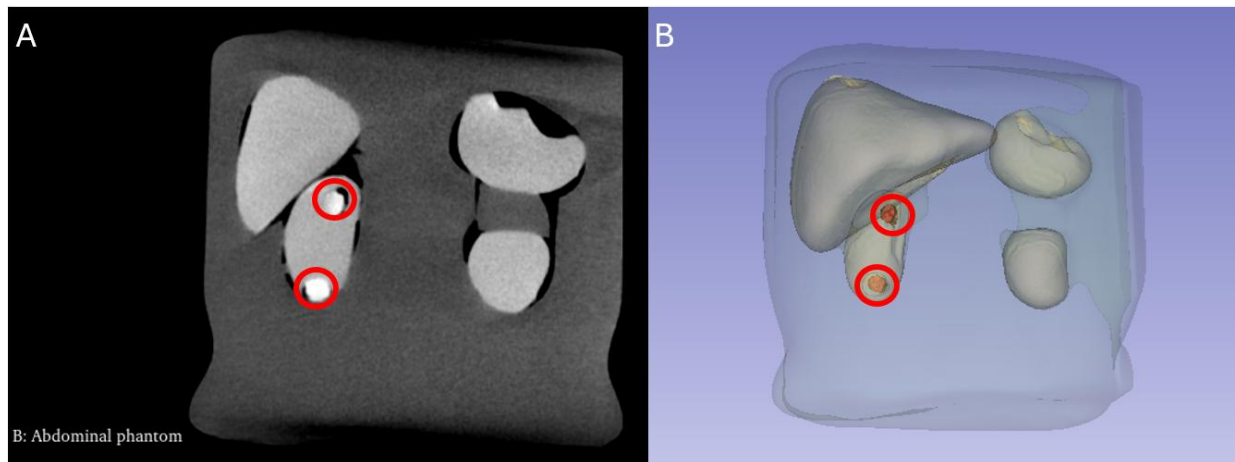


Figure 7. (A) CT image of the abdominal phantom, (B) 3D reconstruction of the CT image. The tumors are seen in the red circles.

Table 1. List of KI concentrations of the simulated tumors and their mean HU values.

KI concentration	Mean HU
1.0% w/v	204.84 ± 16.66
1.5% w/v	256.48 ± 59.09
2.0% w/v	560.28 ± 83.69
2.5% w/v	637.59 ± 122.34
3.0% w/v	804.23 ± 157.99

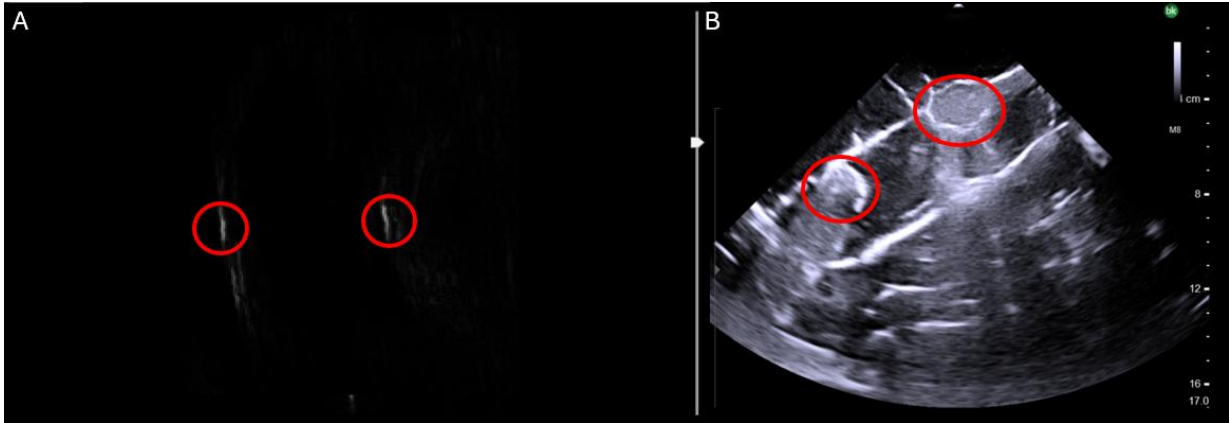


Figure 8. US B-mode images of the abdominal phantom from (A) the GEM5ScD clinical phased array transducer, (B) the 5P1 probe. The red circles highlight tumor phantoms.

4. DISCUSSION AND CONCLUSION

This study presents a deformable, anatomically accurate abdominal phantom fabricated from an agar-gelatin composite and designed from patient CT data to support evaluation of image-guided procedures. The phantom incorporates kidneys, liver, and spleen with embedded renal tumor targets, using KI for CT contrast and psyllium husk for ultrasound contrast to enable multimodal target localization assessment. The phantom was evaluated using both CT and ultrasound imaging modalities. Preliminary results demonstrate clear visualization of the embedded targets in both CT and ultrasound images.

CT focuses on ionizing X-ray attenuation, which increases with atomic number and electron density, thus adding an iodide-based agent increases the photoelectric effect and contrast. Conversely, US uses non-ionizing, high-frequency acoustic waves, which depend on scattering interfaces and impedance mismatches. Psyllium husk powder is utilized due to a better ability to produce backscattering, and overall increasing echogenicity.¹³ Both can be mixed to support dual-modality imaging applications, such as image-guided interventions and deformable registration. Our method facilitates the production of custom, low-cost, deformable phantoms that allow for more variable TMPs, which can significantly enhance system development and validation. Future iterations of the phantom will aim to minimize air gaps between components and improve acoustic properties for ultrasound visualization, while maintaining CT contrast stability.

ACKNOWLEDGMENTS

Research reported in this publication was supported in part by the National Cancer Institute of the National Institutes of Health under Award Number R01CA288379 and by the Cancer Prevention and Research Institute of Texas (CPRIT) under Award Number RP240289 and RP240542. The content is solely the responsibility of the authors and does not necessarily represent the official views of the National Institutes of Health.

REFERENCES

- [1] C. K. McGarry, L. J. Grattan, A. M. Ivory *et al.*, "Tissue mimicking materials for imaging and therapy phantoms: a review," *Phys Med Biol*, 65(23), (2020). <https://www.doi.org/10.1088/1361-6560/abbd17>.
- [2] A. Leibinger, A. E. Forte, Z. Tan *et al.*, "Soft Tissue Phantoms for Realistic Needle Insertion: A Comparative Study," *Ann Biomed Eng*, 44(8), 2442-2452 (2016). <https://www.doi.org/10.1007/s10439-015-1523-0>.
- [3] A. Jawli, W. Aldehani, G. Nabi, and Z. Huang, "Tissue-Mimicking Material Fabrication and Properties for Multiparametric Ultrasound Phantoms: A Systematic Review," *Bioengineering (Basel)*, 11(6), (2024). <https://www.doi.org/10.3390/bioengineering11060620>.
- [4] X. Zhong, P. Zhou, Y. Zhao *et al.*, "A novel tissue-mimicking phantom for US/CT/MR-guided tumor puncture and thermal ablation," *Int J Hyperthermia*, 39(1), 557-563 (2022). <https://www.doi.org/10.1080/02656736.2022.2056249>.
- [5] T. Z. Pavan, E. L. Madsen, G. R. Frank *et al.*, "A nonlinear elasticity phantom containing spherical inclusions," *Phys Med Biol*, 57(15), 4787-804 (2012). <https://www.doi.org/10.1088/0031-9155/57/15/4787>.
- [6] M. Volk, I. Vogt, M. Georgiades *et al.*, "Modulating CT Attenuation of Polyvinyl Alcohol Cryogels for Individualized Training Phantoms in Interventional Radiology: A Proof-of-Concept Study," *Gels*, 11(8), (2025). <https://www.doi.org/10.3390/gels11080664>.
- [7] M. Kraft, S. Ryger, B. P. Berman *et al.*, "Towards a barrier-free anthropomorphic brain phantom for quantitative magnetic resonance imaging: Design, first construction attempt, and challenges," *PLoS One*, 18(7), e0285432 (2023). <https://www.doi.org/10.1371/journal.pone.0285432>.
- [8] M. Zhao, M. Zhou, X. Cao *et al.*, "Stable tissue-mimicking phantoms for longitudinal multimodality imaging studies that incorporate optical, CT, and MRI contrast," *J Biomed Opt*, 28(4), 046006 (2023). <https://www.doi.org/10.1117/1.JBO.28.4.046006>.
- [9] J. Young, M. Shahedi, J. D. Dormer *et al.*, "A low-cost PVC-based dual-modality kidney phantom," *Proc. SPIE 12034, Medical Imaging 2022: Image-Guided Procedures, Robotic Interventions, and Modeling*, 12034Q, (4 April 2022); <https://www.doi.org/10.1117/12.2611592>.
- [10] M. Kim, S. Im, I. Park *et al.*, "Fabrication of agar-based tissue-mimicking phantom for the technical evaluation of biomedical optical imaging systems," *Current Applied Physics*, 61, 80-85 (2024). <https://www.doi.org/10.1016/j.cap.2024.02.013>.
- [11] R. Gautam, D. Mac Mahon, G. Eager *et al.*, "Fabrication and characterization of multi-biomarker optimized tissue-mimicking phantoms for multi-modal optical spectroscopy," *Analyst*, 148(19), 4768-4776 (2023). <https://www.doi.org/10.1039/d3an00680h>.
- [12] M. Bach, C. Aberle, A. Depeursinge *et al.*, "3D-printed iodine-ink CT phantom for radiomics feature extraction - advantages and challenges," *Med Phys*, 50(9), 5682-5697 (2023). <https://www.doi.org/10.1002/mp.16373>.
- [13] L. W. Hofstetter, L. Fausett, A. Mueller *et al.*, "Development and characterization of a tissue mimicking psyllium husk gelatin phantom for ultrasound and magnetic resonance imaging," *Int J Hyperthermia*, 37(1), 283-290 (2020). <https://www.doi.org/10.1080/02656736.2020.1739345>.